Circuit Bounds on Stochastic Transport in the Lorenz equations

Scott Weady,[1] Sahil Agarwal,[1] Larry Wilen,[1] and J. S. Wettlaufer[1,2,3]
[1] *Yale University, New Haven, USA*
[2] *Mathematical Institute, University of Oxford, Oxford, UK*
[3] *Nordita, Royal Institute of Technology and Stockholm University, SE-10691 Stockholm, Sweden**
(Dated: December 14, 2017)

In turbulent Rayleigh-Bénard convection one seeks the relationship between the heat transport, captured by the Nusselt number, and the temperature drop across the convecting layer, captured by Rayleigh number. The maximal heat transport for a given Rayleigh number is the central experimental quantity and the key prediction of variational fluid mechanics in the form of an upper bound. Because the Lorenz equations act a simplified model of turbulent Rayleigh-Bénard convection, it is natural to ask for their upper bounds, which have not been viewed as having the same experimental counterpart. Here we describe a specially built circuit that is the experimental analogue of the Lorenz equations and compare its output to the recently determined stochastic upper bounds of the Lorenz equations [1]. In the chaotic regime, the upper bounds do not increase monotonically with noise amplitude, as described previously [1]. However, because the circuit is vastly more efficient than computational solutions, we can more easily examine this result in the context of the optimality of stochastic fixed points. Finally, because of the control one has with the circuit, an offset in the system allows us to find and examine bifurcation phenomena unique to the electronic analogue.

I. INTRODUCTION

The Lorenz equations are an archetype for key aspects of nonlinear dynamics, chaos and a range of other phenomena that manifest themselves across all fields of science, particularly in fluid flow [see e.g., 2, 3]. Lorenz [4] derived his model to describe a simplified version of Saltzman's treatment of finite amplitude convection in the atmosphere [5]. The three coupled Lorenz equations, which initiated the modern field we now call chaos theory, are

$$\begin{aligned} \dot{x} &= \sigma(y-x) \\ \dot{y} &= \rho x - xz - y \quad \text{and} \\ \dot{z} &= xy - \beta z, \end{aligned} \tag{1}$$

where x describes the intensity of convective motion, y the temperature difference between ascending and descending fluid and z the deviation from linearity of the vertical temperature profile. The parameters are the Prandtl number σ, the normalized Rayleigh number, $\rho = \frac{\mathrm{Ra}}{\mathrm{Ra}_c}$, where $\mathrm{Ra}_c = \frac{27\pi^4}{4}$, and the aspect ratio β. Here we take $\sigma = 10$ and $\beta = \frac{8}{3}$, the original values used by Lorenz.

The sensitivity of solutions to small perturbations in initial conditions and/or parameter values characterize chaotic dynamics and have a wide array of implications. Chaotic behavior does not lend itself well to standard analysis, and modern computational methods provide us with powerful tools to analyze systems that are vastly more powerful than the Royal McBee LGP-30 electronic computing machine that Lorenz used. However, one powerful mathematical method used for example in the study of fluid flows is variational, and assesses the optimal value of a transport quantity, or a bound [6–8], which we briefly discuss next.

A. Bounds on Fluid Flows

Bounding quantities in fluid flows has important physical consequences and substantial theoretical significance. Whereas variational principles are central when an action is well-defined and phase space volume is conserved, they pose significant challenges for dissipative nonlinear systems in which the phase space volume is not conserved and thus not Hamiltonian [e.g., 9]. However, initiated by the work of Howard [10], who used a variational approach to determine the upper bounds on heat transport in statistically stationary Rayleigh-Bénard convection, with incompressibility as one of the constraints, the concept of mathematically bounding the behavior of a host of flow configurations has developed substantially [8], as well as in other dissipative systems such as solidification [11].

Pètrelis and Pètrelis [12] used the background method [7] to produce bounds on the energy dissipation and transport for the Lorenz system. Souza and Doering [13] improved their result producing sharp upper bounds on transport $\langle xy \rangle \leq \beta(\rho - 1)$, which are saturated by the nontrivial equilibrium solutions $(x, y, z) = (\pm\sqrt{\beta(\rho-1)}, \pm\sqrt{\beta(\rho-1)}, \rho - 1)$. Agarwal and Wettlaufer [1] extended the background method to the stochastic Lorenz system, recovering the bounds of Souza and Doering [13] in the zero noise amplitude limit. Here we discuss an experimental approach to this work by building and studying an electronic circuit implementation of the stochastic Lorenz system. This circuit provides us with a simple physical model for transport in Rayleigh-Bènard convection, where $\langle xy \rangle$ models the Nusselt number. Beyond its experimental interest, the circuit

* john.wettlaufer@yale.edu

can perform computations much more efficiently than numerical simulations, a finding that is especially powerful when studying long-time average behavior.

II. THE CIRCUIT LORENZ EXPERIMENT

A. Upper Bounds of the Stochastic Lorenz System

As a model of atmospheric convection for which it was first derived, the Lorenz system might be best described as a *motif*. However, such physically based models can often become more realistic by adding a stochastic element to account for random fluctuations, observational error, and unresolved processes. This conceptually old idea has become particularly popular in climate modeling and weather prediction [e.g., 14, 15]. Here, we follow this approach in the Lorenz system by adding a stochastic term with a constant coefficient [1] viz.,

$$\begin{aligned} \dot{x} &= \sigma(y-x) + A\xi_x \\ \dot{y} &= \rho x - xz - y + A\xi_y \quad \text{and} \\ \dot{z} &= xy - \beta z + A\xi_z, \end{aligned} \tag{2}$$

where A is the noise amplitude and σ, β, and ρ are as in Eq. (1).

The circuit described below in §II B allows us to experimentally test and analyze stochastic bounds of the transport in the Lorenz system subject to forced and intrinsic noise. In the infinite time limit, the stochastic upper bounds of Agarwal and Wettlaufer [1] are given by

$$\langle xy \rangle \leq \beta(\rho - 1) + \frac{A^2}{\rho - 1}\left(1 + \frac{1}{2\sigma}\right). \tag{3}$$

For $A = 0$ these reduce to the upper bounds of Souza and Doering [13]. However, unlike the deterministic case, the fixed point solutions are no longer optimal in the sense that the equilibria are never truly attained. We note that these bounds tend to infinity as $\rho \to 1$, although Fantuzzi [16] made a correction in this low Rayleigh number regime.

B. The Lorenz Electrical Circuit

The Lorenz system can be modeled in an analog circuit through a series of op-amp integrators and voltage multipliers (Fig. 1). Adding a noise element to the integrators allows us to adapt this circuit to the stochastic model. To generate noise we use Teensy 3.5 microprocessors with digital to analog converters. Equipped with "true" analog random number generators, these microprocessors can be modified to generate consistent and finely tunable Gaussian white noise at a very low cost, making them suitable for both educational and experimental purposes. To ensure this noise is symmetric about 0V, we first pass the signals through an AC coupler and then amplify the signal.

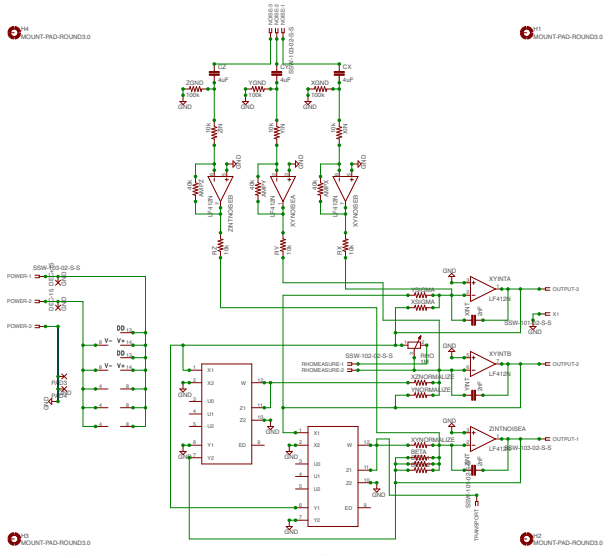

FIG. 1. Schematic of the stochastic Lorenz circuit.

To collect voltage data from the circuit, we use an Arduino Due microprocessor with 12-bit analog read resolution along with several voltage dividers and amplifiers to put the voltages in the Arduino's range of 0-3.3V. When processed, the voltages appear as an integer between 0 and 4095, corresponding to a voltage between 0-3.3V. From this data we can convert back to the original voltage using measurements of the amplifiers and voltage dividers and scaling by 10, the normalization factor of the circuit.

The rate of integration is determined by the three capacitors on the schematic labeled XINT, YINT, and ZINT, which we denote here by C_x, C_y and C_z. This allows us to adjust the sampling rate depending on the application. For measuring transport, we can run the circuit at a very high speed and sample as fast as possible, approximately every 100μs with the Arduino Due. Figure 2 shows samples of the circuit-generated attractor for noise amplitudes $A = 0$ and $A = 4$. We note that these amplitudes are chosen in reference to a baseline voltage and do not numerically correspond to the same amplitude in Eqs. 2.

A key feature of the circuit is the ability to sample xy directly from the evolution equation for z equation. Not only does this provide much faster convergence of $\langle xy \rangle$, but keeping a running average avoids the need to store large arrays of data or perform extra arithmetic operations.

III. THE OFFSET LORENZ SYSTEM

Any analog circuit is subject to asymmetry due to offsets in op-amps and multipliers and imprecise measure-

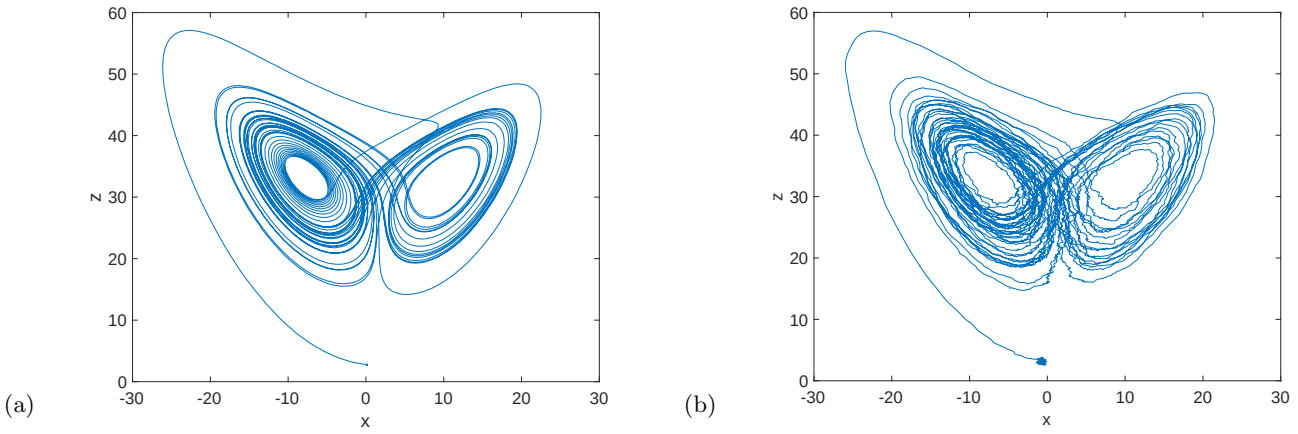

FIG. 2. Circuit generated stochastic Lorenz attractor in the $x-z$ plane for (a) $A=0$ and, (b) $A=4$.

ments of resistors and capacitors. Because the Lorenz system is symmetric under the transformation $(x,y,z)\mapsto(-x,-y,z)$, this poses an issue for our model. To account for this asymmetry we propose a slightly modified model of the Lorenz system described here and analyze its properties.

For the MPY634 multipliers, the transfer function is given by $[(X_1-X_2)(Y_1-Y_2)/10+(Z_1-Z_2)]$, where X_1, X_2, Y_1, Y_2, Z_1 and Z_2 are differential inputs. We assume $Z_1-Z_2=0$, which is a reasonable for our circuit, as both the Z_1 and Z_2 ports are connected to ground, and the terms in the multiplication are precise, namely $(X_1-X_2)=x$, and similarly for the other variables. So the only error we attribute to the multipliers is the output noise, which is 2% at room temperature as listed on the datasheet, and hence we suggest adding normally distributed random variables ε_{xy} and ε_{xz} with zero mean and variance 0.2 to the products xy and xz respectively. However, for simplification, we neglect this in the following discussion.

For the integrators, we model the offset with a slight amplification or dampening factor, which absorbs any small constant voltage offsets. Formally, we say

$$\int_{C_x}\dot{x}dt=(1+\eta_x)\ x$$
$$\int_{C_y}\dot{y}dt=(1+\eta_y)\ y \quad \text{and}$$
$$\int_{C_z}\dot{z}dt=(1+\eta_z)\ z$$

where $\int_{C_i} dt$ corresponds to the actual output of the circuit integrator and η_x, η_y, and η_z are small parameters with absolute value less than 1. Substituting these into the deterministic Lorenz equations (1) we get

$$\begin{aligned}\dot{x}&=\sigma\big[(1+\eta_y)\ y-(1+\eta_x)\ x\big]\\ \dot{y}&=\rho(1+\eta_x)\ x-(1+\eta_x)(1+\eta_z)\ xz-(1+\eta_y)\ y\\ &\text{and}\\ \dot{z}&=(1+\eta_x)(1+\eta_y)\ xy-\beta(1+\eta_z)\ z,\end{aligned}\tag{4}$$

which we refer to as the offset Lorenz system.

A. Equilibria & Stability

To analyze the stability of the offset Lorenz system we take $\eta_x=\eta_z=\eta$ and $\eta_y=-\eta$ where $|\eta|<1$. This is motivated by the fact that the circuit propagates a voltage corresponding to $-y$ rather than $+y$. For simplicity, assume $\varepsilon_{xy}=\varepsilon_{xz}=0$. With these assumptions the offset Lorenz equations become

$$\begin{aligned}\dot{x}&=\sigma\big[(1-\eta)\ y-(1+\eta)\ x\big]\\ \dot{y}&=\rho(1+\eta)\ x-(1+\eta)^2\ xz-(1-\eta)\ y\\ &\text{and}\\ \dot{z}&=(1+\eta)(1-\eta)\ xy-\beta(1+\eta)\ z\end{aligned}\tag{5}$$

We first determine the equilibrium solutions ($\dot{x}=\dot{y}=\dot{z}=0$), and from the evolution equation for x we have $(1+\eta)x=(1-\eta)y$, which yields

$$y=\Big(\frac{1+\eta}{1-\eta}\Big)x.$$

Substituting this into the evolution equation for y we get

$$\rho(1+\eta)x-(1+\eta)^2xz-(1+\eta)x=0,$$

which gives

$$(1+\eta)x\ \big[\rho-(1+\eta)z-1\big]=0,$$

and hence

$$x = 0 \quad \text{or} \quad z = \frac{1}{1+\eta}(\rho - 1).$$

Clearly, if $x = 0$ we get $y = 0$ and $z = 0$. Now upon substitution of z into the evolution equation for z we find

$$\left(\frac{1+\eta}{1-\eta}\right)(1+\eta)(1-\eta)x^2 - \beta(1+\eta)\ \frac{1}{1+\eta}(\rho-1)$$
$$= x^2(1+\eta)^2 - \beta(\rho-1) = 0,$$

and hence

$$x = \pm\frac{1}{1+\eta}\sqrt{\beta(\rho-1)}, \tag{6}$$

so that the nontrivial fixed points are

$$\begin{aligned} x^*_\pm &= \pm\frac{1}{1+\eta}\sqrt{\beta(\rho-1)} \\ y^*_\pm &= \pm\frac{1}{1-\eta}\sqrt{\beta(\rho-1)} \quad \text{and} \\ z^*_\pm &= \frac{1}{1+\eta}(\rho-1), \end{aligned} \tag{7}$$

where $|\eta| < 1$. Note that these solutions are no longer symmetric, but they reduce to the non-trivial fixed points of the standard Lorenz system when $\eta = 0$.

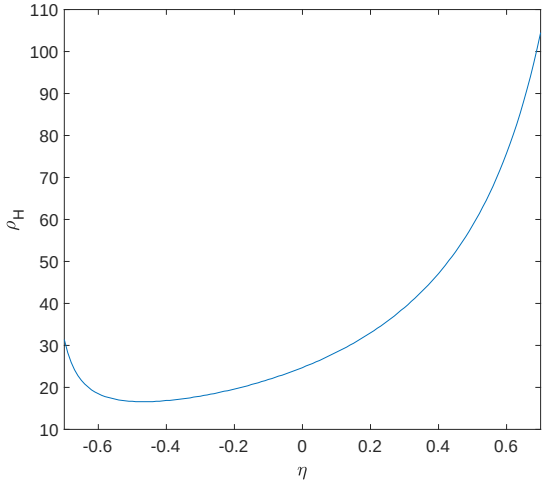

FIG. 3. Bifurcation value as a function of η. The y intercept occurs at $(\eta, \rho_H) = (0, 24.74)$ as expected.

1. *Stability of the Equilibrium Solutions*

The Jacobian for our offset system is given by

$$J(x,y,z) = \begin{pmatrix} -\sigma(1+\eta) & \sigma(1-\eta) & 0 \\ \rho(1+\eta) - (1+\eta)^2\ z & -(1-\eta) & -(1+\eta)^2\ x \\ (1+\eta)(1-\eta)\ y & (1+\eta)(1-\eta)\ x & -\beta(1+\eta). \end{pmatrix}$$

At the trivial equilibrium (x^*_0, y^*_0, z^*_0) the Jacobian is

$$J(0,0,0) = \begin{pmatrix} -\sigma(1+\eta) & \sigma(1-\eta) & 0 \\ \rho(1+\eta) & -(1-\eta) & 0 \\ 0 & 0 & -\beta(1+\eta) \end{pmatrix}$$

This matrix has three negative eigenvalues for $\rho < 1$ and one positive eigenvalue for $\rho > 1$. Hence, as in the standard Lorenz equations, the origin becomes unstable at $\rho = 1$.

Now we compute the Jacobian at (x^*_+, y^*_+, z^*_+), where we take the solution with the positive square root, to get

$$J(x^*,y^*,z^*) = \begin{pmatrix} -\sigma(1+\eta) & \sigma(1-\eta) & 0 \\ \rho(1+\eta) - (1+\eta)(\rho-1) & -(1-\eta) & -(1+\eta)\sqrt{\beta(\rho-1)} \\ (1+\eta)\sqrt{\beta(\rho-1)} & (1-\eta)\sqrt{\beta(\rho-1)} & -\beta(1+\eta) \end{pmatrix}$$

The eigenvalues in their analytical form are cumbersome, so we determine them numerically and find that as in the standard Lorenz system, there is a Hopf bifurcation ρ_H, here with a dependence on η. We find that there is a smooth dependence of ρ_H on η, as can be seen in the numerical solutions in Fig. 3.

2. *Numerical Solutions of the Offset Lorenz System*

We confirm the existence of a Hopf bifurcation for our modified system using numerical solutions. For $\eta = 0.2$, our solutions predict that the bifurcation occurs at $\rho_H \approx 33$. Figures 4 and 5 show numerical simulations of the offset Lorenz system slightly below and above this value respectively. We see that the trajectory does indeed become chaotic.

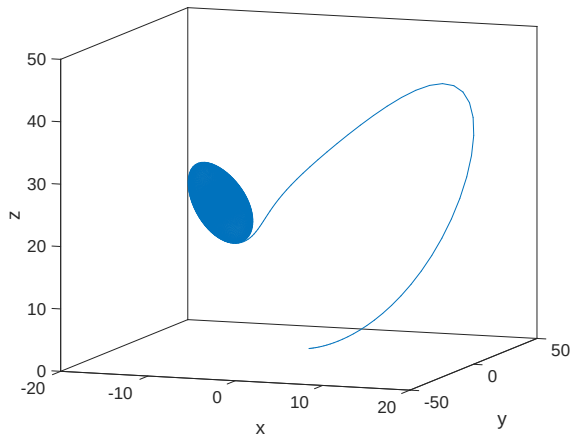

FIG. 4. Plot in (x, y, z) phase space of numerical simulation of the offset Lorenz system at $(\eta, \rho) = (0.2, 31.5)$.

It is important to emphasize that our discussion of the offset Lorenz system has implications for the circuit model. Most notably, it implies the transition to chaos will occur at a different value of ρ than in the standard Lorenz equations, depending on the offset in our op-amp

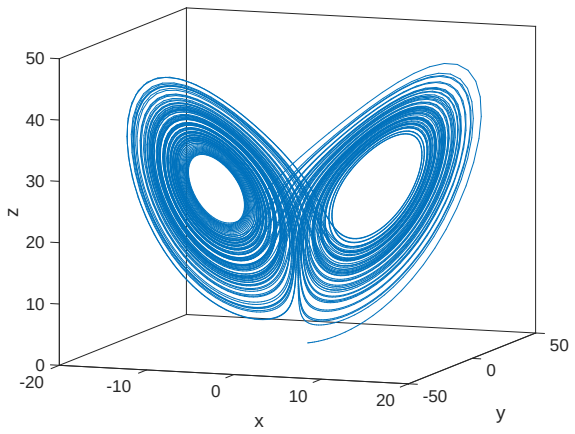

FIG. 5. Plot in (x, y, z) phase space of numerical simulation of the offset Lorenz system at $(\eta, \rho) = (0.2, 33)$.

integrators. The circuit does in fact demonstrate this, with the transition to chaos occurring at $\rho \approx 34$ for $C_{int} = 0.262\mu$F, where C_{int} is the capacitor that controls the speed of integration. Lower capacitance reduces the value of ρ at which the transition to chaos occurs.

IV. RESULTS & DISCUSSION

A. Stochastic Upper Bounds

Using the circuit, we reproduce the results of Agarwal and Wettlaufer [1] for the stochastic upper bounds. Figure 6 shows an average of the transport over three trials for 19 values of ρ and 5 noise amplitudes, including $A = 0$. The results are numerically asymptotic to the analytical upper bounds, until the transition to chaos at $\rho \approx 34$, which is consistent with the analytical work to which we compare our approach. From Equation (6) we see that when we take the product $x^*_\pm y^*_\pm$ we get

$$x^*_\pm y^*_\pm = \frac{1}{1-\eta^2}\sqrt{\beta(\rho-1)},$$

which has $O(\eta^2)$ error versus $O(\eta)$ for the individual coordinate offsets. In light of this we see that despite the delayed transition to chaos and the circuit's asymmetry, the behavior of transport versus Rayleigh number remains approximately the same.

At subcritical Rayleigh numbers we find that, in the circuit, transport tends to *decrease* with noise, in contrast to the increasing stochastic upper bounds. Beyond the transition to chaos however, the increase or decrease of transport with noise amplitude at a given Rayleigh number depends largely on the sampling frequency, number of realizations, and even further by sampling resolution. This has some interesting implications. Unlike numerical methods, the circuit solves the Lorenz equations in real time. Therefore, when we sample xy from the circuit, we are in fact sampling from the full attractor, not just at set discrete time steps. This may provide a view into the realism of ergodicity, especially considering the intrinsic perturbations of the circuit. Nonetheless our sampling only shows convergent values of $\langle xy \rangle$ at very low amplitudes, and this is most likely a result of the resolution rather than the circuit's actual reflection of the chaotic set. Hence, we find that the behavior of the circuit at high Rayleigh number is no different from the numerics, both of which show that noise is indistinguishable from chaos.

B. Noise and Unstable Periodic Orbits

As we increase the noise amplitude, the relationship between transport and ρ becomes increasingly linear, smoothing out the jump at the transition to chaos. This behavior suggests the existence of a critical noise amplitude, namely, the minimum amplitude at which this occurs. Taking advantage of the circuit's computational speed, we can quantify this more rigorously. When we fix ρ and plot transport as a function of amplitude, we see a trend. For $\rho < \rho_H$, transport tends to decrease with noise amplitude until a critical value is reached, after which it increases linearly on average. If we take a moving average over the full curve and record the amplitude corresponding to the minimum, we find that this amplitude achieves a maximum near the homoclinic orbit where $\rho \approx 13.96$. Mathematically the existence of a homoclinic orbit implies the existence of unstable periodic orbits embedded in phase space. The decreasing transport behavior that we see corresponds to dissipation as the state of the system passes near these periodic trajectories, which are coupled to the noise amplitude.

V. CONCLUSION

Circuits modeling dynamical systems have largely been used for pedagogical purposes. However, much less work has utilized these models for actual computation and analysis. Our study of the Lorenz circuit demonstrates the value of using analog circuits to study dynamical systems from a variety of perspectives, a key one being as a model for transport in turbulent Rayleigh-Bènard convection.

Ultimately, an analog circuit forms a dynamical system that can be modeled by a set of differential equations. Solving the inverse problem – constructing a circuit to fit a given set of equations – reveals the possibility of using circuits to analyze a variety of dynamical systems of both mathematical and physical interest. Basic models have been constructed for dynamical systems such as the van der Pol oscillator and the Rössler system. However, with the aid of machine printed circuits we may

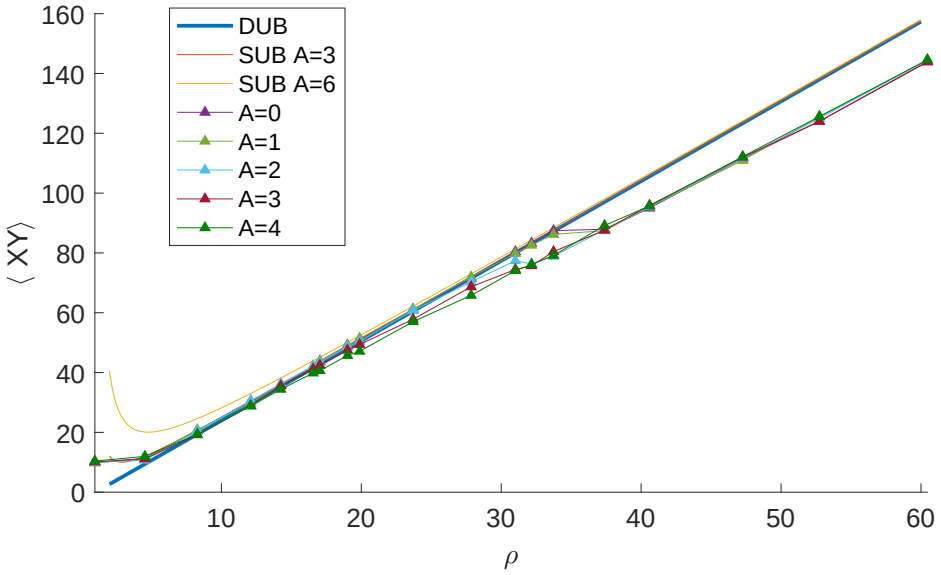

FIG. 6. The transport $\langle xy \rangle$ versus ρ for circuit solutions. The transition to chaos occurs at $\rho \approx 34$.

be able to model much more complex systems extending from neuronal networks to geophysical flows. Indeed, because numerical methods suffer from a wide range of instabilities, large memory requirements, and high computational costs, analog circuits eliminate these issues, offering a new and efficient way to study quantitative and qualitative behavior and experimentally test analytical theories and closure schemes.

VI. ACKNOWLEDGEMENTS

All of the authors thank Yale University for support. SA and JSW acknowledge NASA Grant NNH13ZDA001N-CRYO for support. JSW acknowledges Swedish Research Council Grant 638-2013- 9243 and a Royal Society Wolfson Research Merit Award for support.

[1] S. Agarwal and J. S. Wettlaufer, Phys. Lett. A **380**, 142 (2016).
[2] D. Ruelle, *Elements of Differential Dynamics and Bifurcation Theory.* (Academic Press, San Diego, 1989).
[3] S. H. Strogatz, *Nonlinear Dynamics and Chaos: With Applications to Physics, Biology, Chemistry, and Engineering*, 2nd ed. (Westview Press, 2014).
[4] E. N. Lorenz, J. Atmos. Sci. **20**, 130 (1963).
[5] B. Saltzman, J. Atmos. Sci. **19**, 329 (1962).
[6] L. N. Howard, Annu. Rev. Fl. Mech. **4**, 473 (1972).
[7] C. R. Doering and J. D. Gibbon, *Applied analysis of the Navier-Stokes equations*, Cambridge Texts in Applied Mathematics, Vol. 12 (Cambridge University Press, 1998).
[8] R. R. Kerswell, Physica D: Nonlinear Phenomena **121**, 175 (1998).
[9] G. J. Sussman and J. Wisdom, *Structure and Interpretation of Classical Mechanics* (MIT Press, Boston, MA, 2001).
[10] L. N. Howard, J. Fluid Mech. **17**, 405 (1963).
[11] A. J. Wells, J. S. Wettlaufer, and S. A. Orszag, Phys. Rev. Lett. **105**, 254502 (2010).
[12] F. Pètrelis and N. Pètrelis, Phys. Lett. A **326**, 85 (2004).
[13] A. Souza and C. R. Doering, Phys. Lett. A **379**, 518 (2015).
[14] H. M. Arnold, I. M. Moroz, and T. N. Palmer, Phil. Trans. R. Soc. A **371** (May 28, 2013).
[15] N. Chen and A. J. Majda, Proc. Natl. Acad. Sci. USA **114**, 1468 (2017).
[16] G. Fantuzzi, in *2015 Program of Study: Stochastic Processes in Atmospheric and Oceanic Dynamics, Woods Hole Oceanographic Institution Tech. Rep. WHOI-2016-05*, edited by J. S. Wettlaufer and O. Bühler (Woods Hole Oceanographic Institution, 2016) pp. 188–226.